A Simplified Biosphere Model for Global Climate Studies

Y. XUE, P. J. SELLERS, J. L. KINTER AND J. SHUKLA

Center for Ocean–Land–Atmosphere Interactions, Department of Meteorology, University of Maryland, College Park, Maryland

(Manuscript received 8 February 1990, in final form 7 November 1990)

ABSTRACT

The Simple Biosphere Model (SiB) as described in Sellers et al. is a bio-physically based model of land surface–atmosphere interaction. For some general circulation model (GCM) climate studies, further simplifications are desirable to have greater computation efficiency, and more important, to consolidate the parametric representation. Three major reductions in the complexity of SiB have been achieved in the present study.

The diurnal variation of surface albedo is computed in SiB by means of a comprehensive yet complex calculation. Since the diurnal cycle is quite regular for each vegetation type, this calculation can be simplified considerably. The effect of root zone soil moisture on stomatal resistance is substantial, but the computation in SiB is complicated and expensive. We have developed approximations, which simulate the effects of reduced soil moisture more simply, keeping the essence of the biophysical concepts used in SiB.

The surface stress and the fluxes of heat and moisture between the top of the vegetation canopy and an atmospheric reference level have been parameterized in an off-line version of SiB based upon the studies by Businger et al. and Paulson. We have developed a linear relationship between Richardson number and aerodynamic resistance. Finally, the second vegetation layer of the original model does not appear explicitly after simplification. Compared to the model of Sellers et al., we have reduced the number of input parameters from 44 to 21. A comparison of results using the reduced parameter biosphere with those from the original formulation in a GCM and a zero-dimensional model shows the simplified version to reproduce the original results quite closely. After simplification, the computational requirement of SiB was reduced by about 55%.

1. Introduction

Since Charney's (1975) pioneering study, several experiments have shown that variations in land surface characteristics can have a significant impact on the climate. The atmosphere is sensitive to the surface albedo, soil moisture, roughness, and other surface characteristics on many time scales (Charney et al. 1977; Shukla and Mintz 1982; Rind 1984; Sud et al. 1988).

In order to understand these interactions, not only qualitatively but also quantitatively, more realistic surface parameterizations than those used in the above studies are required. Since the 1970s, considerable progress in understanding surface micrometeorology has been achieved through theoretical work and observations from field experiments.

The results of these studies have been incorporated in simple models of the biosphere which have then been coupled to general circulation models (GCM) of the Earth's atmosphere (Dickinson et al. 1986; Sellers et al. 1986). These models are more physically and biologically realistic than the preexisting land surface parameterizations used in GCMs. Using these models, some experiments have been carried out to investigate Amazon deforestation (Dickinson and Henderson-Sellers 1988; Shukla et al. 1990), and African desertification (Xue et al. 1990). These studies show that the vegetation canopy is an important factor for determining the surface energy budget. Some conclusions, for example, the surface warming due to deforestation or desertification, were not found using less realistic models.

The Simple Biosphere Model (SiB) of Sellers et al. (1986) is intended to realistically simulate the controlling biophysical processes. It includes three soil layers and two vegetation layers. The model attempts to provide a more accurate diurnally varying description of the surface energy partition into sensible heat and latent heat. Vegetation canopy processes include the resistances to evapotranspiration and heat flux, and the effect on the interception loss.

The simple biosphere is linked to the GCM atmosphere through fluxes of radiation, sensible and latent heat, and momentum. By comparison with most of other GCMs, SiB is more complex in the treatment of the surface albedo, surface energy and soil moisture and requires many more input parameters. The specification and calibration of these parameters and the sensitivity of the calculated surface energy balance to these have been presented in Sellers and Dorman (1987) and in Sellers et al. (1989), respectively. It was found that SiB produced generally good simulations of the observed time series of latent, sensible and

Corresponding author address: Dr. Yong-Kang Xue, Center for Ocean–Land–Atmosphere Interactions, 2213 Comp. & Space Science Bldg., College Park, MD 20742-2425.

ground heat fluxes and surface radiative fluxes. Sato et al. (1989) implemented SiB into the Center for Ocean–Land–Atmosphere Interaction (COLA) Global Spectral Model (Kinter et al. 1988). The comparative performance of the GCM using SiB and a "bucket hydology" (Manabe 1969) was presented by Sato et al. (1989).

The SiB was also used to study Amazon deforestation by Shukla et al. (1990). While it has been shown to be an improvement over the "bucket" hydrology for simulation of the hydrologic cycle and the surface energy partition, it has some limitations for application to extended-range prediction and climate studies. Most notable is that the large number of parameters whose values are only approximately known for many vegetation types makes sensitivity testing and model validation difficult. The values of many of the parameters are scarce for different biomes in different parts of the world.

There are thousands of grid cells over the earth's land surface in a high resolution GCM. A grid cell typically encloses an area of several tens of thousands of square kilometers. Thus, the land surface characteristics specified in a grid cell are average values taken over large areas. Even if only one biome is present in a given grid cell, its form and physiological characteristics can vary considerably. This and the limitations of computer time and available surface data, make it imperative that the surface soil–vegetation model be as simple as possible. The large number of parameters also prohibits identification of the dominant physical mechanisms. On the other hand, SiB's foundation on biophysical principles and the totality of empirical data that exist make it conceptually attractive. We have analyzed the SiB equations to identify the dominant parameter over realistic ranges of the environmental conditions and to simplify the parameterizations and, where possible, the structure of SiB.

The SiB model includes the calculation of radiation fluxes, aerodynamic resistance, and surface resistance. We will discuss the simplification of these three parameterizations in sections 2, 3, and 4, respectively. The simplification of the SiB structure is discussed in section 5, and some results from numerical experiments are discussed in section 6 for the zero-dimensional model and section 7 for the GCM. For the purposes of this discussion, hereafter we shall refer to the model of Sellers et al. (1986) as SiB, and our simplified version of SiB as SSiB.

2. Radiation fluxes

One of the main influences of the land surface on the surface radiation budget is through the albedo; see for example, Charney (1975). Typically the surface albedo is prescribed in a GCM in accordance with observations. The specified albedo values are the mean values over a certain time period (e.g., Matthews 1985). However, in order to have a better understanding of the diurnal cycle of the surface energy balance, a more precise calculation of diurnal variation of albedo is required.

The diurnal variation of albedo noted in micrometeorological studies is seldom applied in GCMs because of its complexity. The basis of the radiation transfer equations in SiB were originally presented by Dickinson (1983) and Sellers (1985) explored a method for integrating the existing formulations that describe the interception of radiation by individual leaves over whole canopies. The comparison between observations and the model results is fairly good in spite of some simplifying assumptions in the model. The process of calculating the diurnal variation of albedo is quite complex and can be computationally expensive when the "two stream method" is applied at every grid point and every time step in a GCM integration.

The diurnal variation (maximum to minimum) of surface albedo typically amounts to about 0.05 when the cosine of solar zenith angles change from about 1 to 0.02, between the local times of about 0800 and 1700 local time. When the cosine of solar zenith angle is less than 0.02, the changes of albedo can be large but the solar flux is much less, so any error in calculating albedo at these times does not cause a significant error in the computed surface energy balance. The shape of the diurnal variation of surface albedo is very regular in the SiB results, and a quadratic fit is adequate to reduce the complex calculation.

The albedo is mainly controlled by the spectral and angular distribution of solar radiation incident on the surface, (i.e., direct or diffuse, infrared or visible), the surface conditions as determined by vegetation and soil, the solar zenith angle, and snow cover. For a specific wavelength and vegetation type, the albedo of the direct radiation is a function of solar zenith angle and snow cover. We used the SiB radiation formulation to calculate the diurnal variation once for each vegetation type, then obtained the coefficients for empirical quadratic equations.

Where vegetation communities exist, radiative transfer processes at the surface are quite complicated. In order to know the surface energy balance, not only the reflection but also the interception, transmission, and absorption of radiation by vegetation should be calculated. These terms also vary diurnally. The fitting of albedo is therefore not sufficient. Instead of fitting each aforementioned variable, we parameterized the surface albedo as well as the net absorbed radiation at canopy (F_c) and at ground (F_{gs}) which are directly used in the surface energy balance equation.

The surface net radiation is given by the sum of the terms R_{nc} and R_{ngs}, which refer to the canopy and the ground components, respectively,

$$R_{nc} = F_c - 2\sigma_s T_c^4 V_c \delta_t + \sigma_s T_{gs}^4 V_c \delta_t \qquad (1)$$

and

$$R_{ngs} = F_{gs} - \sigma T_{gs}^4 + \sigma_s T_c^4 V_c \delta_t \qquad (2)$$

where F_c and F_{gs} are the sums of the absorbed shortwave and longwave radiation components for the canopy and ground, respectively, σ_s is the Stefan–Boltzmann constant, T_c is the canopy temperature, V_c is the vegetation cover fraction, δ_t is the canopy transmittance for thermal infrared radiation, and T_{gs} is the ground temperature.

Because both albedo and absorption vary diurnally in a similar manner, we use similar equations to parameterize them. The equations for absorption may be written as

$$F_c = [a_1 + b_1 \cos\Theta + c_1 \cos^2\Theta + d_1 v_1 + e_1 v_1^2 + f_1 v_2 + g_1 v_2^2] F^{(0)}_{\Lambda,\mu} \quad (3)$$

and

$$F_{gs} = [a_2 + b_2 \cos\Theta + c_2 \cos^2\Theta + d_2 v_2 + e_2 v_2^2 + f_2 v_2 + f_2 v_2^2] F^{(0)}_{\Lambda,\mu} \quad (4)$$

where Θ is the solar zenith angle, and v_1 and v_2 are the snow cover on the canopy and ground, respectively. The first three terms are for the snow free situation, while others are for snow cover. The radiation interaction of the two snow layers is not considered in this simplification because it is not significant in most cases. The albedos have similar equations with different coefficients.

Using the SiB radiation model we can obtain different albedo and absorption values with different zenith angles and snow covers for different vegetation types. The coefficients in (3) and (4) were computed by the least squares method. The coefficients depend on the vegetation types. As in SiB, we divide the incoming solar and thermal radiation into "visible," near-infrared, and thermal infrared bands. The surface thermal emissivity and absorptance is assumed to be diurnaly invariant. Therefore, the parameterization described above does not apply to this component. The values of these coefficients for different vegetation types and different seasons are shown in Table 1.

Several experiments have been carried out to validate this simplification. We first checked the model performance without snow cover. Figures 1a and 1b show the comparison of albedos and absorptions between SiB and SSiB for vegetation type 2, broadleaf deciduous trees. (There are 12 vegetation types in the SiB model. A detailed presentation can be found in Dorman and Sellers 1989). The variation in the absorption of visible light is almost zero for this vegetation type. For every vegetation type the fitting results of SSiB are good for the snow free case with an rms difference of less than 0.01. Near noon, when solar flux is at a maximum, the fits are quite accurate.

With snow cover the results are still very close to the SiB values for most vegetation types. When two vegetation layers are used, the radiative interaction between two snow layers becomes more significant than with one layer of vegetation. Figure 1c shows the worst case, which is the comparison of the albedo for vegetation type 10, dwarf trees with ground cover. The snow cover is 0.70 in both layers. Even though this is the worst case, the differences are still not very large. The other two story vegetation types are mainly in tropical and subtropical regions, where there is little snow cover. At this time we have not included more terms to incorporate the interaction of the two stories. SSiB requires about 80% less computer time for the snow free case, and about 40% less for snow covered cases.

3. Stomatal resistance

The evapotranspiration from vegetation is an important process controlling the energy partition at the surface. The rate of transpiration is determined by the stomatal resistance, which depends on the vegetation type and also a number of atmospheric and hydrologic variables affecting the supply of and demand for moisture. The parameterization of the stomatal resistance in SiB is based on Jarvis' (1976) equations for an individual leaf. Sellers (1985) developed a method to calculate the bulk canopy resistances from Jarvis' equations using an integration of the light-dependent part of the resistance for all leaf orientations and for the whole canopy. With the help of a leaf angle distribution function, an analytic expression was obtained. The equation for surface resistance, r_c, during the daytime is (Sellers et al. 1989)

$$\frac{1}{r_c} = \frac{V_c N_c}{Kc}\left[\frac{b}{fF\pi(0)} \ln\left\{\frac{\mu f e^{-kL_{tc}} + G(\mu)}{\mu f + G(\mu)}\right\} - \ln\left\{\frac{\mu f + G(\mu)e^{-kL_{tc}}}{\mu f + G(\mu)}\right\}\right] F(\Sigma), \quad f = \frac{a + bc}{cF\pi(0)}. \quad (5)$$

At nighttime some vegetations types do not stop transpiring. Following a similar procedure to Sellers et al. (1988), while photosynthetically active radiation (PAR) is zero, we have

$$\frac{1}{r_c} = V_c N_c \frac{0.5}{(a/b) + c} L_{tc} F(\Sigma) \quad (6)$$

where V_c is the vegetation cover, N_c the greenness of the vegetation, a, b and c are species dependent PAR response constants, $F_\pi^{(0)}$ is PAR flux above the canopy, L_{tc} the local leaf area index of canopy, K the extinction coefficient, μ the cosine of the PAR flux zenith angle, and $G(\mu_\pi)$ is leaf angle projection in the direction μ_π given by the semi-empirical formulation of Goudriaan (1977). The constants a, b, c and $G(\mu_\pi)$ depend on vegetation type. These data are given in Dorman and Sellers (1989). Here $F(\Sigma)$ is the product of all stress terms:

TABLE 1a. Coefficients of radiation absorption.

	Visible				Near infrared			
	Direct				Direct			
Type	*a*	*b*	*c*	Diffuse	*a*	*b*	*c*	Diffuse
				January				
2 canopy	0.6767	−1.2498	0.8561	0.2905	0.5185	−0.9075	0.6205	0.2370
2 ground	0.2381	1.2803	−0.8824	0.6283	0.2638	1.0428	−0.7258	0.5748
7 canopy	0.6826	−0.6360	0.1153	0.3542	0.1555	−0.1285	0.0155	0.0852
7 ground	0.1405	0.8621	−0.2539	0.5361	0.3017	0.7779	−0.3617	0.5883
				April				
2 canopy	0.7017	−0.1528	−0.0201	0.6276	0.4343	0.0994	−0.0823	0.4163
2 ground	0.2169	0.2267	−0.0263	0.3110	0.2350	0.2979	−0.0974	0.3420
7 canopy	0.7418	−0.4242	−0.0553	0.4776	0.1931	−0.0826	−0.0320	0.1315
7 ground	0.1095	0.5951	−0.0356	0.4261	0.2638	0.6303	−0.2011	0.5168
				July				
2 canopy	0.6957	0.0817	−0.0600	0.7167	0.4573	0.3141	−0.1979	0.5457
2 ground	0.2227	−0.0038	0.0118	0.2232	0.1959	0.0067	0.0106	0.2003
7 canopy	0.7762	0.2563	−0.3139	0.8134	0.3069	0.3460	−0.2751	0.3876
7 ground	0.0988	−0.1125	0.2472	0.1066	0.1271	0.0260	0.1884	0.1798

TABLE 1b. Coefficients of albedo.

Type		*a*	*b*	*c*	*d*	*e*	*f*	*g*
					January			
2 visible	direct	0.0852	−0.0306	0.0264	0.1443	0.0457	0.3867	0.0189
2 visible	diffuse	0.0812			0.1403	0.0390	0.4025	0.0200
2 near IR	direct	0.2177	−0.1353	0.1053	0.0000	0.0000	0.0956	0.0008
2 near IR	diffuse	0.1882			0.0000	0.0000	0.1002	0.0008
7 visible	direct	0.1769	−0.2260	0.1386	0.1819	0.0601	0.2367	0.0274
7 visible	diffuse	0.1097			0.1808	0.0386	0.2861	0.0342
7 near IR	direct	0.5428	−0.6493	0.3462	−0.1795	0.0232	0.0818	0.0028
7 near IR	diffuse	0.3264			−0.1382	0.0166	0.0970	0.0034
					April			
2 visible	direct	0.0814	−0.0740	0.0464	0.0876	0.1469	0.2035	0.0075
2 visible	diffuse	0.0614			0.1263	0.1438	0.1959	0.0058
2 near IR	direct	0.3307	−0.3073	0.1797	−0.0459	0.0044	0.0530	0.0004
2 near IR	diffuse	0.2417			−0.0490	0.0045	0.0509	0.0003
7 visible	direct	0.1487	−0.1709	0.0909	0.1366	0.0803	0.2309	0.0322
7 visible	diffuse	0.0963			0.2048	0.0694	0.2050	0.0268
7 near IR	direct	0.5431	−0.5477	0.2332	−0.1552	0.0258	0.0810	0.0033
7 near IR	diffuse	0.3517			−0.1714	0.0261	0.0732	0.0029
					July			
2 visible	direct	0.0815	−0.0778	0.0482	0.0640	0.1597	0.1726	0.0000
2 visible	diffuse	0.0601			0.1119	0.1558	0.1726	0.0000
2 near IR	direct	0.3468	−0.3207	0.1873	−0.0555	0.0072	0.0438	0.0000
2 near IR	diffuse	0.2540			−0.0598	0.0072	0.0438	0.0000
7 visible	direct	0.1250	−0.1438	0.0667	0.0783	0.1712	0.0728	0.0012
7 visible	diffuse	0.0799			0.1879	0.1482	0.0714	0.0006
7 near IR	direct	0.5661	−0.3720	0.0867	−0.2761	0.0879	0.0222	0.0002
7 near IR	diffuse	0.4326			−0.2916	0.0828	0.0213	0.0001

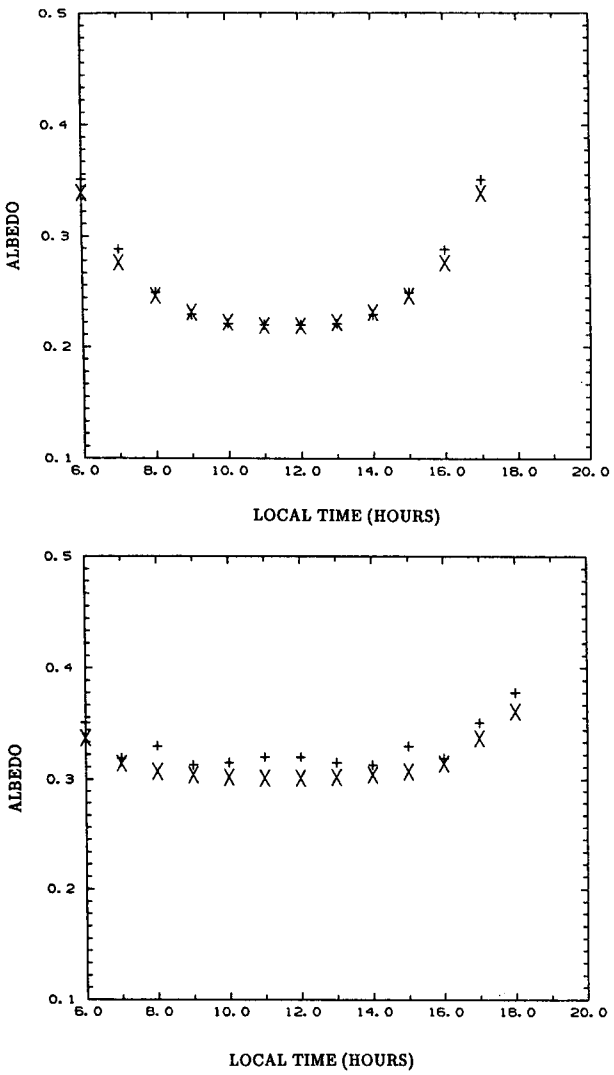

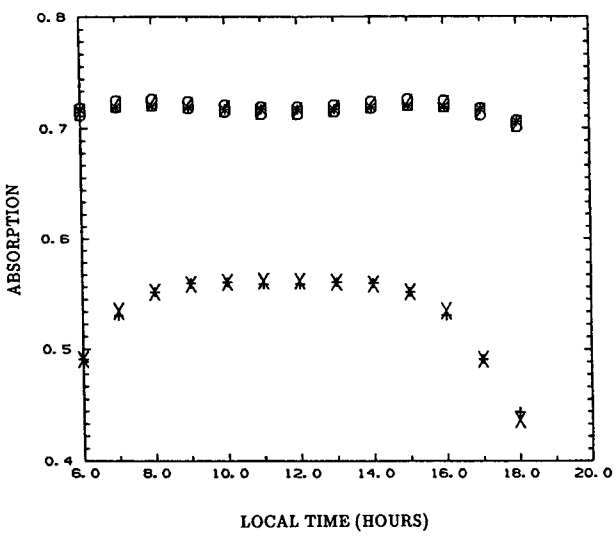

FIG. 1. (a) Comparison of SiB and SSiB albedos for broadleaf deciduous trees. X: SiB albedo, +: SSiB albedo. (b) Comparison of SiB and SSiB absorption values for broadleaf deciduous trees. X: SiB near-infrared, +: SSiB near-infrared, *: visible SiB, O: SSiB visible. (c) Comparison of SiB and SSiB albedo values for dwarf trees with ground cover. The snow cover is 0.70 in both layers. X: SiB, +: SSiB.

$$F(\Sigma) = f(\psi)f(T)f(T_a, e_a) \tag{7}$$

where $f(\psi)$, $f(T)$, and $f(T_a, e_a)$ are the adjustment factors for the soil water deficit, leaf temperature, and atmospheric water vapor pressure deficit, respectively; T_a and e_a are the temperature and water vapor pressure in the canopy air space. The soil moisture effect becomes very important only when the soil is dry. However, the calculation of this effect is the most complex part. There have been several attempts to develop some simple equations which relate stomatal resistance to soil moisture. Based upon observations, several empirical relations have been developed; some of which are exponential functions and some are linear ones (Szeicz et al. 1973; Dolman 1988; Stewart 1988). The method in SiB is based on equations presented in Federer (1979) which are comprehensive and general, but are complex and computationally expensive.

The equation in SiB is (Sellers et al. 1986)

$$f(\psi) = \frac{\psi_L - \psi_{c2}}{\psi_{c1} - \psi_{c2}} \tag{8}$$

where ψ_L is the leaf water potential, ψ_{c2} is the leaf water potential at which stomata close completely, and ψ_{c1} is the leaf water potential at which stomata start to close. The leaf water potential is obtained from related soil and vegetation properties, which require a large number of parameters. Moreover, since ψ_L is also related to the transpiration rate, which depends upon the stomatal resistances, the whole calculation process is fairly complex.

In order to simplify this part, we test the sensitivity of stomatal resistance to soil moisture based upon Federer's equations first. We use a zero-dimensional version of SiB, that is, a version of SiB driven by atmospheric data observed a short distance above the surface. With different initial soil moisture values we ran the SiB model for several days so that the soil moisture

changed as a function of simulated time. Figure 2a shows the results from this experiment for vegetation type 1, tropical rainforest. The abscissa is the logarithm of the negative of the soil water potential ψ_r. The different symbols represent the results from different days. Comparing the relationship between soil moisture and $f(\psi)$, we found the resistance in this model decreases very sharply after soil moisture falls below a critical value. This is in agreement with previous studies. We noted that $f(\psi)$ varied exponentially with the soil moisture. For other vegetation types, we did similar experiments and found similar results. Using the results from SiB we developed empirical equations relating soil moisture and stomatal resistance for each vegetation type.

TABLE 2. The coefficients of c_1 and c_2.

		c_1	c_2
TYPE1	Broadleaf-evergreen trees	1.2	6.25
TYPE2	Broadleaf-deciduous trees	5.35	5.57
TYPE3	Broadleaf and needleaf trees	1.92	5.73
TYPE4	Broadleaf-evergreen trees	3.7	5.53
TYPE5	Needleleaf-deciduous trees	7.8	5.66
TYPE6	Broadleaf trees with groundcover	1.8	5.67
TYPE7	Groundcover only	1.73	5.80
TYPE8	Broadleaf shrubs with perennial groundcover	3.0	5.98
TYPE9	Broadleaf shrubs with bare soil	1.39	6.37
TYPE10	Broadleaf shrubs with ground cover	0.96	5.37
TYPE11	Bare soil		
TYPE12	Winter wheat and broadleaf-deciduous trees	0.58	4.36

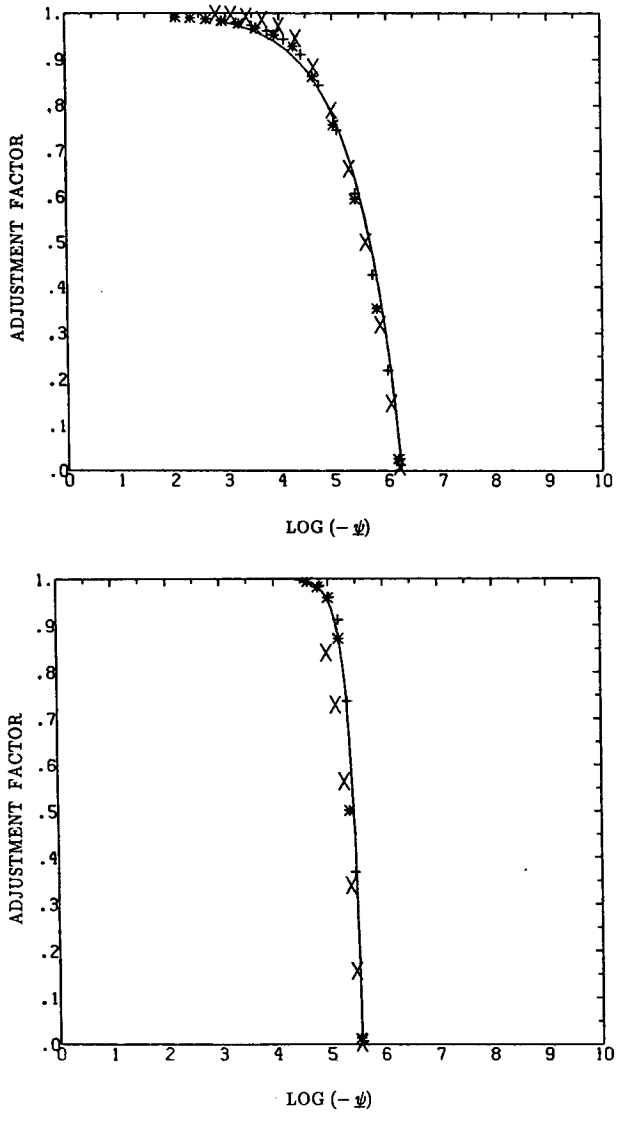

FIG. 2. (a) The dependence of the adjustment factor $f(\psi)$ and soil water potential for tropical rainforest, the results from SSiB are shown as —. The results from SiB for the 5th, 10th, and 15th day are shown as X, *, and +, respectively. (b) Same as Fig. 2a, except for broadleaf deciduous trees.

$$f(\psi) = 1 - e^{-c_2[c_1 - \ln(-\psi_r)]} \tag{9}$$

where ψ_r is the soil water potential and c_1 and c_2 depend on vegetation type and are obtained by a least square method to fit the results in these experiments. The values for different vegetation types are given in Table 2. c_1 represents the point at which stomates close completely, and c_2 is a slope factor. We feel these kinds of conceptual parameters might be more meaningful in the global climate study than some real vegetation quantities, such as root volume.

Using different atmospheric observational data, we carried out the same tests and found that the values of c_1 and c_2 have only slight differences. The forcing data had no significant effect on these values. The results from Eq. (9) are also shown in Fig. 2a. They are very close to the original results. The rms error is 0.0062 for type 1 and of the same magnitude for other types.

For some vegetation types the change of $f(\psi)$ is more dramatic. Figure 2b shows the same results for type 2. Although this curve is more nearly linear, Eq. (9) still provides a good fit. Note that the stress terms for temperature and water vapor deficit are very simple in SiB. These equations can be found in Sellers et al. (1986) and have not been changed in SSiB.

4. Aerodynamic resistances

The vertical eddy flux transfer above the reference height is calculated using the Mellor–Yamada second-order closure scheme in SiB–GCM (Mellor and Yamada 1982). Transfer between the vegetated surface and the reference height is complicated and has not been extensively studied in the context of GCM simulation work. Sellers et al. (1986, 1989) developed equations to calculate aerodynamic resistances within and above vegetation. While the derivations are comprehensive and complex, their usage in a GCM is relatively simple.

Unlike conventional GCMs, where a single areodynamic resistance is specified in the lowest layer, there

are three aerodynamic resistances in SiB: r_d, the resistance between the soil surface and the canopy air space; r_b, the resistance between all of the canopy leaves and the canopy air space; and r_a, the resistance between the canopy air space and the reference height, see Fig. 3. The bulk boundary layer resistance r_b (Sellers et al. 1986) given by

$$\frac{1}{r_b} = \frac{\sqrt{u}}{c_b} + \frac{\bar{L}_l}{890}\left(\frac{T_c - T_a}{l}\right)^{1/4} \tag{10}$$

and the resistance from the soil surface to the canopy source height r_d is

$$r_d = \frac{c_d}{u\psi_H} \tag{11}$$

$$\psi_H = \left[1 + 9g\frac{T_{gs} - T_a}{T_{gs}u^2} Z_2\right]^{1/2} \tag{12}$$

where l is the turbulent length scale, Z_2 the height of canopy top, g the acceleration due to gravity, u the wind speed at the top of vegetation, and c_b and c_d are coefficients, which depend on the vegetation types. The calculation of c_b and c_d is discussed in Sellers et al. (1986).

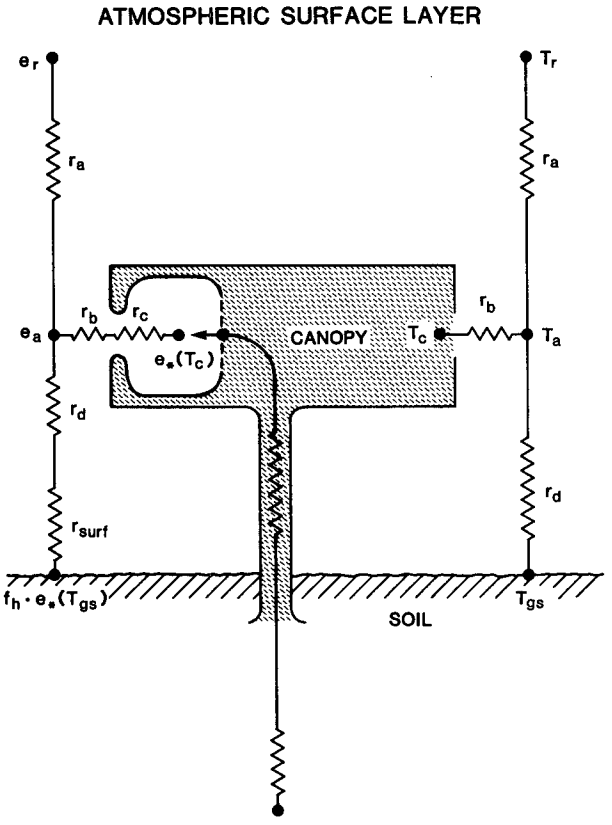

FIG. 3. Schematic diagram of SSiB. T_r is the air temperature at reference height, T_c the canopy temperature, T_a the air temperature within the canopy space, T_g the soil temperature, r_a the aerodynamic resistance between canopy air space and reference height, r_b the bulk boundary layer resistance, r_c the bulk stomatal resistance, r_d aerodynamic resistance between canopy air space and ground.

In a GCM, it is necessary to obtain u from u_r, the wind speed at reference height. A complete consideration for this relation should include the correction of nonneutral stability conditions. However, from experiments we found this consideration not only complicates the computation procedure, but also makes the solution unstable. For simplicity, we use neutral conditions to obtain u from u_r, which yields

$$u = u_r - \frac{u_*}{k_0}\left[\ln\frac{Z-d}{Z_0}\right]\Bigg|_{Z_l}^{Z} - \frac{G_2 u_*}{k_0}\ln\frac{Z-d}{Z_0}\Bigg|_{Z_2}^{Z_l} \tag{13}$$

where u_* is the friction velocity, k_0 the von Kármán constant, Z_m the reference height, Z_0 the roughness length, and d the displacement height. According to observational data (Garratt 1978), estimates of the momentum flux coefficient at Z_2 are 1.5–2.0 times larger than that predicted from extrapolation of the log–linear profile, which is used to describe the variation of wind speed with height within the "constant stress layer" near surface. An adjustment factor G_2, therefore, has been introduced for the resistance between Z_2 and transition height Z_l as in SiB, see Sellers et al. (1989). We take the value of G_2 to be constant for all vegetation types equal to 0.75. Above Z_l a log–linear wind profile was assumed valid. We take $Z_l = Z_2 + 11.785\ Z_0$. Using Eq. (13) r_b may be given by

$$\frac{1}{r_b} = \frac{\sqrt{u_r}}{c_b'} + \frac{L_l}{890}\left(\frac{T_c - T_a}{l}\right)^{1/4}. \tag{14}$$

The second term at the right hand side of Eq. (14) is usually one order of magnitude smaller than first term. It changes slightly with the difference of the temperatures due to the 1/4 power. This term becomes important only when the wind becomes weak. The second term has now been set as a constant to ensure sufficient resistance as u_r goes to zero.

The equation for bulk boundary layer resistance r_b then becomes

$$\frac{1}{r_b} = \frac{\sqrt{u_r}}{c_b'} + c_2'. \tag{15}$$

The parameterization of the resistance between the canopy source height and the reference height, r_a, is based on Monin–Obukhov similarity theory. The equations, which were developed by Paulson (1970) and Businger et al. (1971), have been introduced into the SiB model. Although their formulations have been supported by a large number of measurements and widely used in boundary layer studies, the direct use of these equations in a GCM is extremely time consuming. As a result Sato et al. (1989) did not implement this formulation in SiB–GCM but replaced it with an empirical equation set.

According to Paulson's methods, the equations for the transfer of momentum above the canopy may be written as follows

$$\frac{u_r}{u} = \frac{1}{k_0}\left[\ln\left(\frac{Z_r - d}{Z_0}\right) - \psi_1\right] \tag{16}$$

where the nonneutral correction factor ψ_1 is a function of $(Z - d)/L$ only; L is the Monin–Obukhov length given by

$$L = -u_* c_p \rho T / k_0 g h \tag{17}$$

where c_p is the specific heat at constant pressure, ρ is the air density, T the temperature and h the turbulent heat flux. Following Paulson we define

$$\zeta \equiv \frac{z - d}{L}. \tag{18}$$

When $\zeta < 0$,

$$\psi_1 = \ln\left(\frac{1 + x^2}{2}\right) - \ln\left(\frac{1 + x}{2}\right) + 2\tan^{-1}x - \frac{\pi}{2} \tag{19}$$

$$x = (1 - 16\zeta)^{1/4}; \tag{20}$$

when $\zeta > 0$,

$$\psi_1 = -4.7\zeta. \tag{21}$$

An iteration process has to be used to solve these equations. It is well known from Businger's equations (Businger et al. 1971) that the Richardson number is a unique function of the variable ζ and that the Richardson number is based on the atmospheric static stability. Since in his equations the Richardson number is a complex function of ζ, these equations could only be solved by iteration. Louis (1979) developed equations in which the aerodynamic resistance is a function of Richardson number and surface roughness. His results showed that the unstable cases compared better with exact calculations than the stable cases. In the unstable cases, the simulation results depended on the ratio of height z and surface roughness z_0. The differences are relatively large since z/z_0 varies from 4×10^2 to 2×10^3. Also, since surface roughness varies with different vegetation type and season, different equations

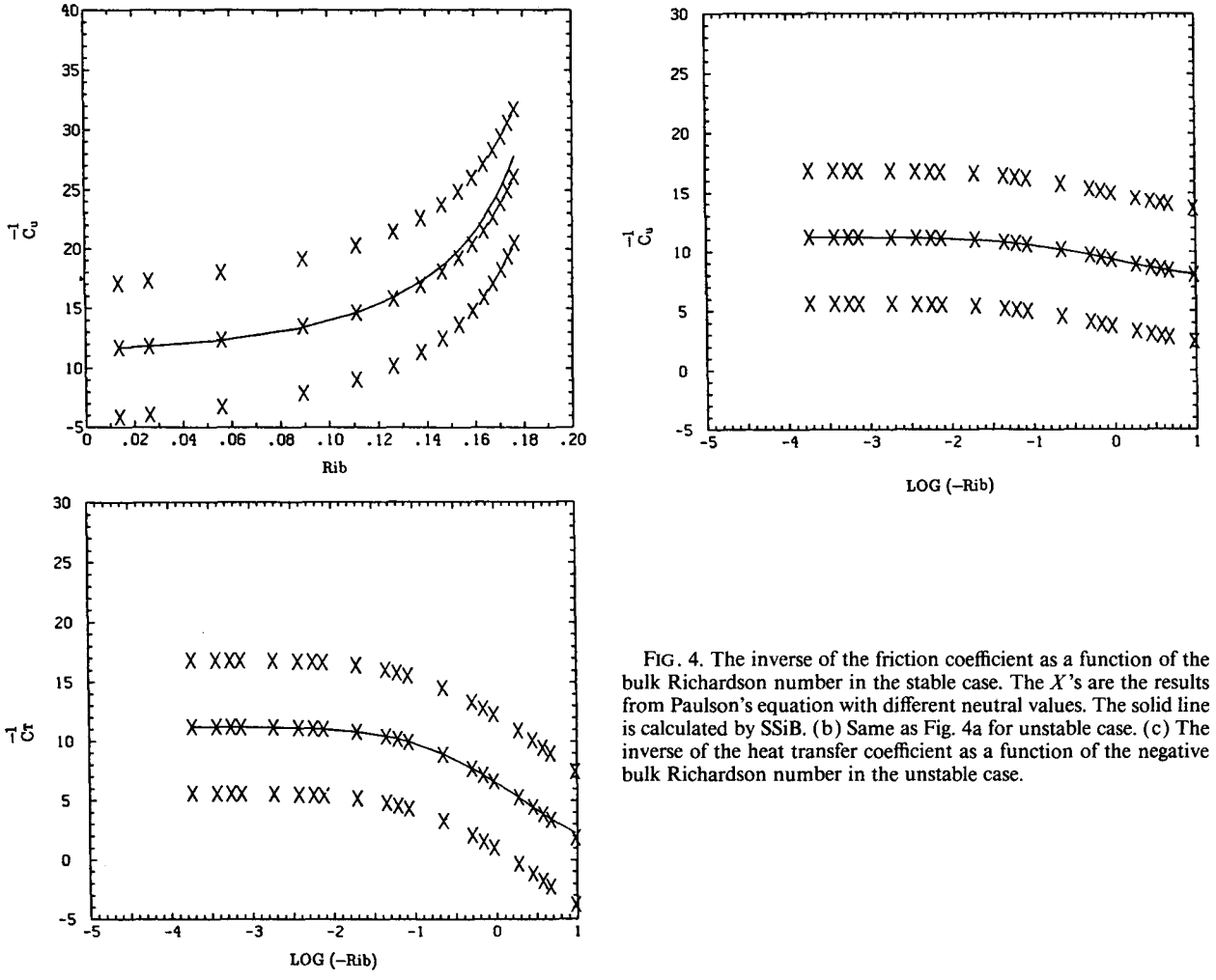

FIG. 4. The inverse of the friction coefficient as a function of the bulk Richardson number in the stable case. The X's are the results from Paulson's equation with different neutral values. The solid line is calculated by SSiB. (b) Same as Fig. 4a for unstable case. (c) The inverse of the heat transfer coefficient as a function of the negative bulk Richardson number in the unstable case.

might be needed for different cases if we tried Louis' scheme in SiB. We have developed a new parameterization, which excludes the neutral part. The non-neutral part depends only on the Richardson number.

We may write Eq. (16) as

$$\frac{U_r}{U_*} = C_{un}^{-1} + C_u^{-1} \tag{22}$$

where the neutral part is given by

$$C_{un}^{-1} = \frac{1}{k_0} \ln\left(\frac{z_r - d}{Z_0}\right), \tag{23}$$

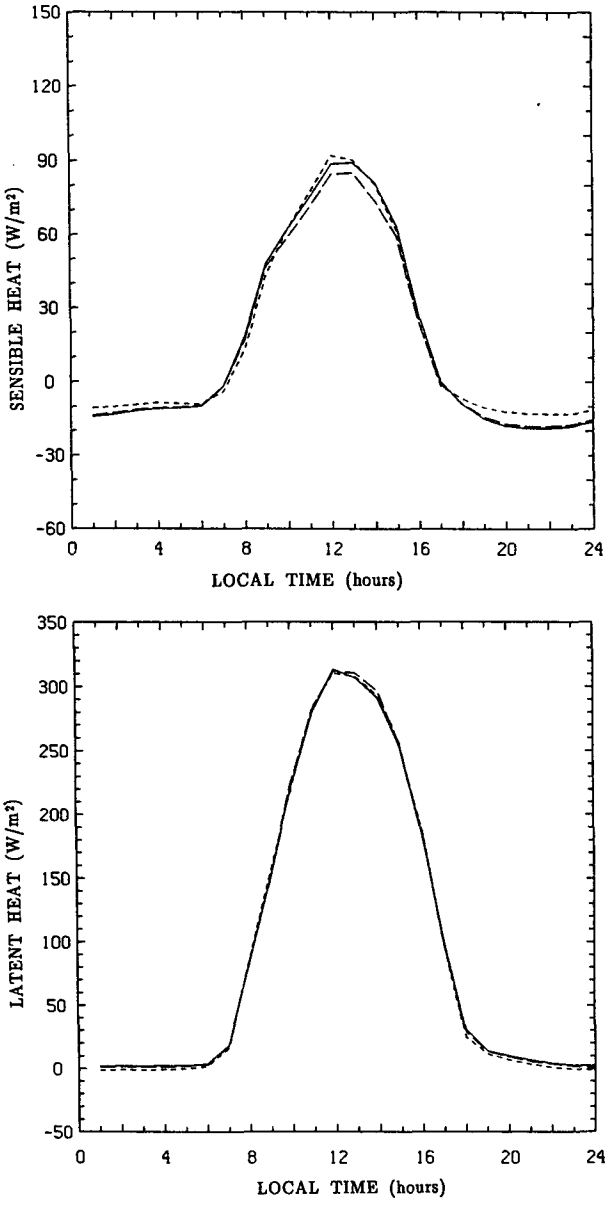

FIG. 5. (a) Predicted values for the three month average diurnal variation of sensible heat flux using Amazon observational data as forcing. Solid: SiB, dashed: exponential r_a-simplification, dotted: linear r_a-simplification. (b) Same as Fig. 5a, except for latent heat flux.

and the nonneutral part can be parameterized by

$$C_{un}^{-1} = \frac{1}{k_0} e^{[0.563(\alpha-0.396)-0.262(\alpha-0.396)^2]}$$

$$\alpha = \log(-\mathrm{Ri}) \quad \text{when } -10 < \mathrm{Ri} < 0 \tag{24}$$

$$C_u^{-1} = C_{u0}/\sinh[20(0.21 - \mathrm{Ri})]$$

$$\text{when } 0.16 > \mathrm{Ri} > 0 \tag{25}$$

$$C_{u0} = 12.10 \tag{26}$$

$$\mathrm{Ri} \equiv \frac{g\Delta Z \Delta\theta}{\theta(\Delta u)^2}$$

where θ is the potential temperature.

The results from these equations are shown in Fig. 4a (stable case) and Fig. 4b (unstable case). When Ri is smaller than -10 or greater than 0.16, C_u^{-1} is taken as a constant. The figure showed that the results from those equations are very close to the iterative solution in both stable and unstable cases.

The nonneutral adjustment to the transfer of heat flux between the heights Z_2 and Z_m, is described by

$$\frac{(T_r - T_a)U_*}{(-\overline{w'\Theta'})} = C_{TN}^{-1} + C_{TT}^{-1} \tag{27}$$

where C_{TN} is the neutral heat transfer coefficient,

$$C_{TT}^{-1} = \frac{-2a}{k_0}[f(x_{Z_m}) + (G_2 - 1)f(x_{z_r}) - G_2 f[x_{z_2}]] \tag{28}$$

$$f(\alpha) = -e^{[b(\alpha+c)+d(\alpha+c)^2]} \quad \text{when } \mathrm{Ri} < 0 \tag{29}$$

where $a = 0.296$, $b = 1.475$, $c = 0.979$, $d = -0.277$, $\alpha = \log(-\mathrm{Ri})$, and

$$C_{TT}^{-1} = C_{u0}^{-1}\left[1 + \frac{Z_r - d}{Z_m - d}(G_2 - 1) - G_2\left(\frac{Z_2 - d}{Z_m - d}\right)\right] \Big/ \sinh[20(0.21 - \mathrm{Ri})] \quad \text{when } \mathrm{Ri} > 0. \tag{30}$$

The result for unstable conditions is shown in Fig. 4c. Whenever we know the Richardson number, r_a can be obtained from Eqs. (28)–(30) as

$$r_a = (C_{TN}^{-1} + C_{TT}^{-1})/U_*. \tag{31}$$

The Richardson number is a function of air temperature within the canopy space, which depends on the aerodynamic resistance, r_a. Although the aforementioned method greatly simplified the calculation, iteration is still required to solve the problem. Based upon the preceding equations, we can make a further simplification.

Each grid point in a GCM is assumed to be the average of the influence of a large number of subgrid-

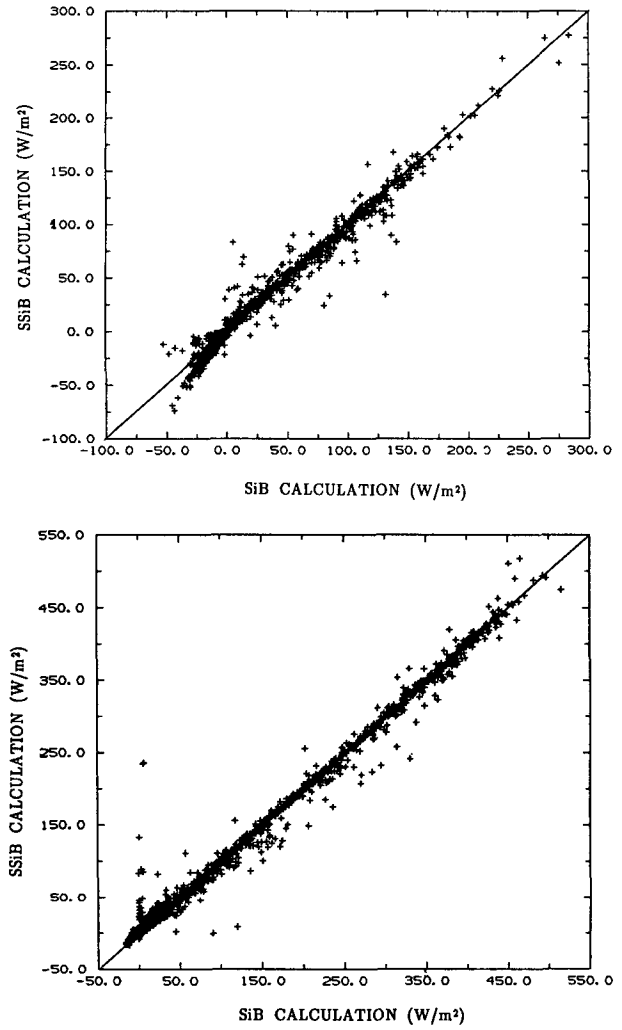

FIG. 6. (a) Comparison of the predicted values of sensible heat flux by SiB and SSiB using Amazon observational data as forcing, from September to November. (b) Same as Fig. 6a, except for latent heat flux.

scale eddies. The distribution of independent variables in a grid point is represented by their mean and standard deviation. Sud and Smith (1984) assumed a Gaussian distribution of the ensemble for the primary independent variables in a grid point and recalculated the relationship between aerodynamic resistances and ensemble mean Richardson number. They showed that this effect had a tendency to change the curve from exponential to linear. Meanwhile, in most cases the atmosphere changes from very stable to free convection quickly. We might be able to use near-linear equations instead of the exponential relations in our GCM experiments for the transfer of momentum. We use

$$C_u^{-1} = \begin{cases} 0.315\ \mathrm{Ri}, & -10 \leqslant \mathrm{Ri} < 0 \quad (32) \\ 66.85\ \mathrm{Ri}, & 0 \leqslant \mathrm{Ri} \leqslant 0.16. \quad (33) \end{cases}$$

TABLE 3. Comparison of the model parameters.

Definintion	SiB	SSiB
Vegetation cover	Vc, Vg	Vc
Leaf angle distribution	Oc, Og	Oc
Height of canopy top	z2	z2
Height of canopy bottom	z1	
Leaf index	Lc, Lg	Lc
Rooting depth	Zdc, Zdg	Zdc
Root length density	Dgc, Dgg	
Root cross section	Rcroc, Rcrog	
Thickness of 3 soil layers	D1, D2, D3	D1, D2, D3
Green fraction	Nc, Ng	Nc
rs coefficients	$(a, b, c)_c$, $(a, b, c)_g$	(a, b, c)
Constant for temperature adjustment	$(T1, Th, To)_c$ $(T1, Th, To)_g$	(T1, Th, To)
Constant for water vapor deficit adjustment	h5c, h5g	h5c
Constant for moisture adjustment	$(\psi_{c2}\psi_{c1})_c$ $(\psi_{c2},\psi_{c1})_g$	(C1, C2)
Root resistance	Rc, Rg	
Plant resistance	*r*(plant)	
Roughness length	zo	zo
Displacement height	*d*	*d*
Soil pore	Os	Os
Soil moisture potential	ψ_s	ψ_s
b parameter	*B*	*B*
Lengthscale of leaf	*l*	
Canopy source height	ha	
Slope	α	α
Parameter for *rd*	Cd	Cd
Parameter for *rb*	Cb	Cb
Parameter for aerodynamic resistance	G1, G2, G3, ZTZO	

For aerodynamic resistance r_a under unstable conditions we used

$$f(\mathrm{Ri}) = 0.904\ \mathrm{Ri} \quad (34)$$

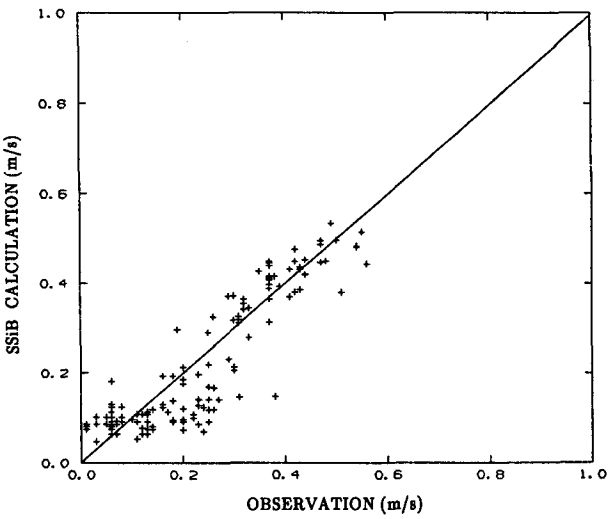

FIG. 7. Comparison of the observed and predicted values of friction velocity for the Amazon from September to November 1979.

to replace Eq. (29). In the stable case we have

$$C_{TT}^{-1} = 66.85\ \mathrm{Ri}\left[1 + \frac{z_r - d}{z_m - d}(G_2 - 1) - G_2\left(\frac{z_2 - d}{z_m - d}\right)\right]. \quad (35)$$

Moreover, the equation for r_a can be written as

$$r_a = \frac{1}{U_m}(C_{TN}^{-1}C_{UN}^{-1} + C_{TN}^{-1}C_{UU}^{-1} + C_{UN}^{-1}C_{TT}^{-1} + C_{TT}^{-1}C_{UU}^{-1}). \quad (36)$$

Since the fourth term on the right-hand side is much smaller than the first three terms, we may eliminate it. Putting Eqs. (32)–(35) into Eq. (36) and considering the energy balance equation

$$\frac{T_a - T_m}{r_a} = \frac{T_c - T_a}{r_b} + \frac{T_{gs} - T_a}{r_d}, \quad (37)$$

and the definition of Richardson number, we have a quadratic equation to obtain r_a, where T_{gs} is the ground temperature. Since r_a is always greater than zero, it is easy to rule out one solution to obtain a unique value.

To test this simplified scheme, we used the observational data from the Amazon rainforest and a Norway spruce forest (Sellers and Dorman 1989) as forcing and integrated the zero-dimensional model for three

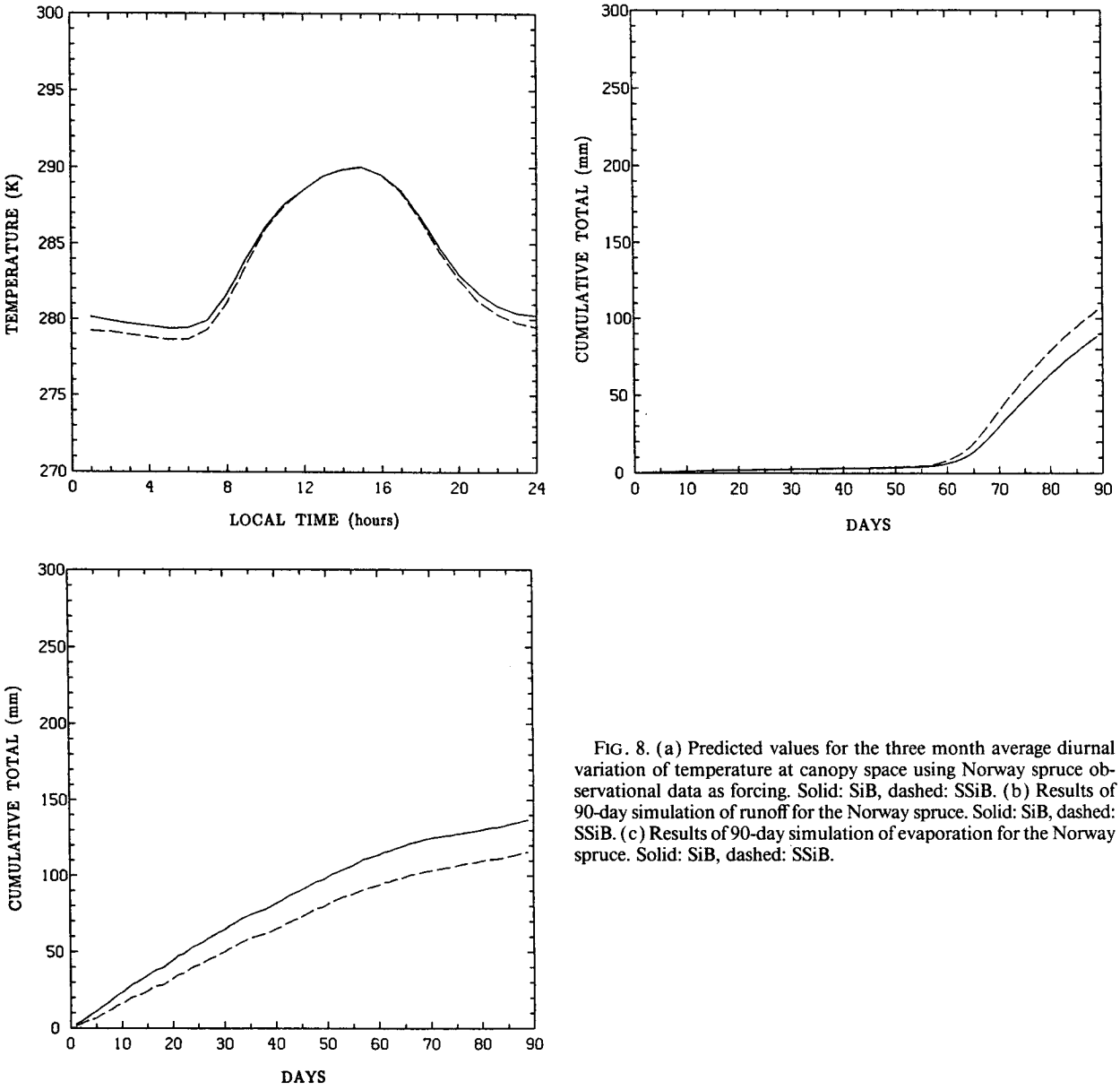

FIG. 8. (a) Predicted values for the three month average diurnal variation of temperature at canopy space using Norway spruce observational data as forcing. Solid: SiB, dashed: SSiB. (b) Results of 90-day simulation of runoff for the Norway spruce. Solid: SiB, dashed: SSiB. (c) Results of 90-day simulation of evaporation for the Norway spruce. Solid: SiB, dashed: SSiB.

months with three different aerodynamic resistance formulations. The results are averaged over three months. Figures 5a and 5b show comparisons of the diurnal variations of latent heat flux and sensible heat flux, respectively, among SiB, exponential r_a-simplification, and linear r_a-simplification using the Amazon rainforest observational data as forcing. The evaporation rates are nearly the same in the three models, while the differences for sensible heat flux are slightly larger. The largest differences in the calculated sensible heat fluxes occur near noon and at night. The root-mean-square (rms) difference of sensible heat flux is about 4.0 W m^{-2} for the exponential, and 3.0 W m^{-2} for the linear approximation. For the latent heat flux the main differences occur at night. The rms is about 3 W m^{-2} for both the exponential and linear simplifications. Figures 6a and 6b compare the values of sensible heat flux and latent heat flux from SiB and SSiB using the linear r_a-description. The points come from the three-month simulations. From these figures we find that SiB and SSiB agree well.

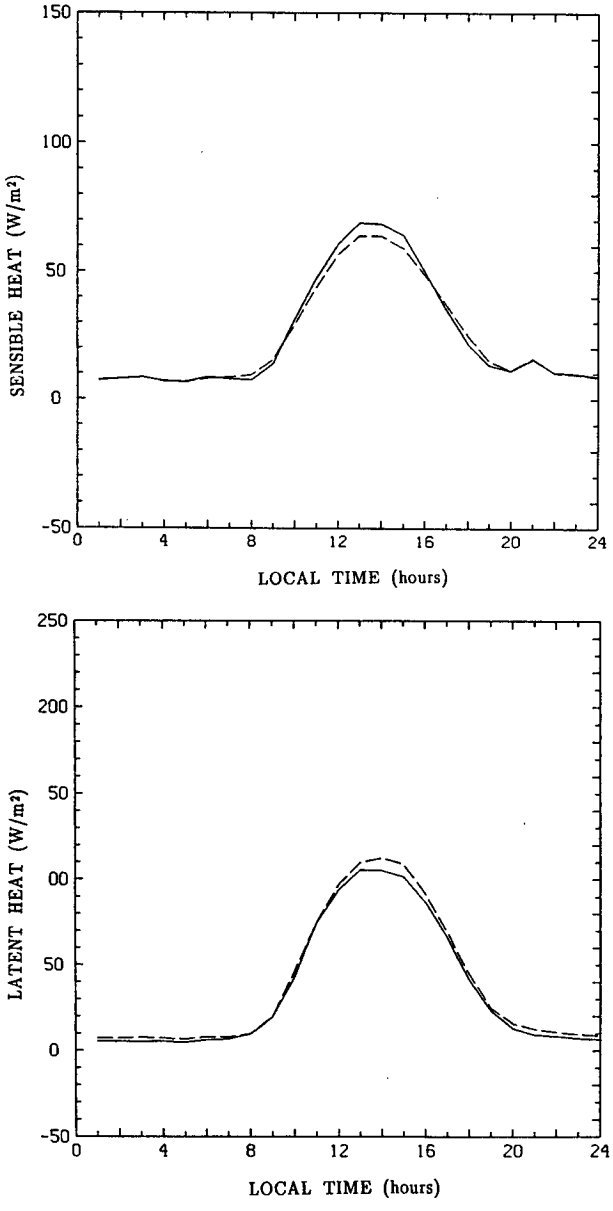

FIG. 9. (a) Predicted values for the three month average diurnal variation of sensible heat flux for dwarf trees with ground cover. The forcing data are from Norway spruce observational data, from July to September. Solid: SiB, dashed: SSiB. (b) Same as Fig. 9a, except for latent heat flux.

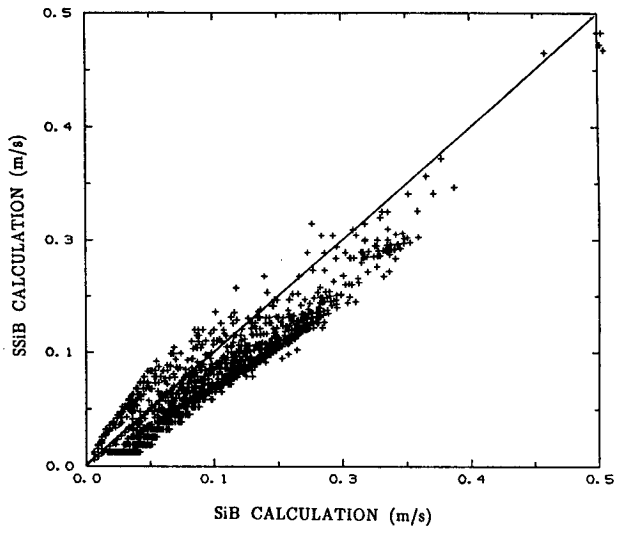

FIG. 10. Comparison of the predicted values of friction velocity between SiB and SSiB for dwarf trees with ground cover. The forcing data are from Norway spruce observational data, from July to September.

The SSiB results for the Norway spruce experiment are even closer to SiB. The relative differences in the total latent heat flux are less than 2% in both exponential and linear approximations, and about 6% for sensible heat flux. The differences are hard to see from the figures.

5. Model structure

There are potentially two vegetation stories in the SiB model. The vegetation types with two layers are broadleaf trees with ground cover (type 6), broadleaf shrubs with ground cover (type 8), dwarf trees and shrubs with ground cover (type 10), and broadleaf-deciduous trees with winter wheat (type 12) (Dorman and Sellers 1989). Most are on the African continent, some in South America, and some near the North Pole. The multilayer model is more realistic and might be easier to compare with the observations, but it requires more parameters and computer time. The interactions between different vegetation layers and between the surface and vegetation should be examined very carefully. More observations might be needed to validate this kind of multilayer system. Here, we use just one layer in SSiB. When reducing the vegetation to one layer from two stories for vegetation types 6, 8, 10, and

12, we tried to reproduce the effects on surface processes simulated by SiB. A number of numerical experiments were carried out to optimize the parameters for one story.

After the simplifications discussed above, SSiB has about half as many parameters as SiB. Table 3 shows the comparison of parameters before and after simplification. The parameters decrease in number from 44 to 21. Among the 23 eliminated parameters, 12 are due to the change of model structure, and another 11 are from the simplification of the parameterizations. Among the 21 parameters in the simplified model, 14 are for vegetation, and 7 are for the soil.

There are seven prognostic equations in this model, which can be regarded as a subset of the original SiB equation set. These equations are presented in the Appendix.

6. Experiments using the simplified 0-D SiB model

Numerous tests have been carried out to validate the SSiB. In this section, we present some results from the zero-dimensional SiB model, for which the required meteorological forcing consists of temperature, water vapor pressure and wind speed at the reference level; precipitation; the downward longwave radiation; and the visible and near-infrared direct and diffuse radiation fluxes. We ran two tests using observations from the Amazon rainforest and Norway spruce field experiments (Sellers and Dorman 1987). When integrating the simple model, the initial data are the same as those used in Sellers and Dorman (1987).

The comparison of SiB and SSiB aerodynamic resistances is discussed in section 4. Figure 7 shows the comparison of friction velocity between observations in the Amazon region and the calculated value from SSiB. The rms error is 0.07 m s^{-1}. The calculated values agree fairly well with observations. Comparing the results in Sellers et al. (1989) Fig. 5b, which is a comparison between SiB and the observations, we find the two models to be very similar.

Figure 8 shows the comparison between SiB and SSiB for the Norway spruce field experiments. Figure 8a compares the T_a (temperature at canopy space) value. Two sets of results are very close; there is less than 1 degree difference between them. Figures 8b and 8c show the cumulative runoff and evaporation. In SSiB the total evaporation decreases by about 21 mm after 90 days integration, while surface runoff increases by about 17 mm.

In both the Amazon rainforest and the Norway spruce cases, the value of soil moisture is high since the precipitation input is large. There is only one vegetation story for these types in SiB. We were not able to use these two datasets to test fully SSiB in dry conditions and for two vegetation stories. Unfortunately, no observational data are available to test the simplifications we made for dry weather and two story biomes. In order to complete the tests in the zero dimensional models, we used data from GCM results as forcing.

In the Congo region the vegetation is also rainforest. The initial soil wetness was dry: 0.22, 0.15, and 0.42, in the three layers. The simplified soil moisture treatment should affect the results for this type. However, the results are similar to the Amazon rainforest and Norwegian spruce cases. The differences between SiB and SSiB are quite small; the evaporation rate in SSiB is about 10 W m^{-2} less while sensible heat flux is larger by about the same amount.

For two story vegetation the impacts of simplification on the model are relatively large. Figures 9a and 9b show the diurnal variation of latent heat flux and sensible heat flux from an experiment in which the Nor-

TABLE 4. The results comparison between SiB and SSiB.

			Evaporation (mm) month			Sensible heat (W mm^{-1}) month			u^* (m s^{-1}) month		
Location	Type	Total	1	2	3	1	2	2	1	2	3
Amazon (S)	1	290.4	3.71	2.96	3.15	17.7	19.4	12.9	.19	.18	.17
Amazon (SS)	1	295.2	3.78	3.01	3.20	16.9	18.6	11.7	.16	.15	.15
Congo (S)	1	185.8	1.79	1.86	2.63	93.2	89.9	68.8	.53	.53	.48
Congo (SS)	1	185.5	1.80	1.82	2.67	93.3	91.3	68.6	.50	.50	.45
Nowegien (S)	4	118.6	1.70	1.51	0.76	24.1	16.2	14.2	.15	.18	.17
Nowegien (SS)	4	123.4	1.67	1.60	0.86	24.6	14.4	13.1	.13	.16	.15
Volta (S)	6	357.6	3.97	3.99	4.35	45.0	43.6	34.8	.73	.70	.60
Volta (SS)	6	336.5	3.43	3.58	4.31	49.1	47.7	32.2	.74	.70	.59
West Sudan (S)	8	215.4	2.46	2.30	2.44	69.5	72.5	68.7	.29	.33	.40
West Sudan (SS)	8	247.1	2.82	2.74	2.77	52.9	56.3	55.3	.25	.30	.38
Chad (S)	8	122.0	0.71	1.74	0.74	78.3	70.4	74.9	.33	.39	.37
Chad (SS)	8	122.5	0.70	1.72	0.73	73.2	65.9	71.1	.32	.37	.36
Amazon (S)	9	269.3	3.91	2.71	2.65	12.1	29.5	32.4	.23	.21	.21
Amazon (SS)	9	267.5	3.68	2.77	2.63	19.0	27.8	29.7	.24	.21	.21

S: SiB.
SS: SSiB.

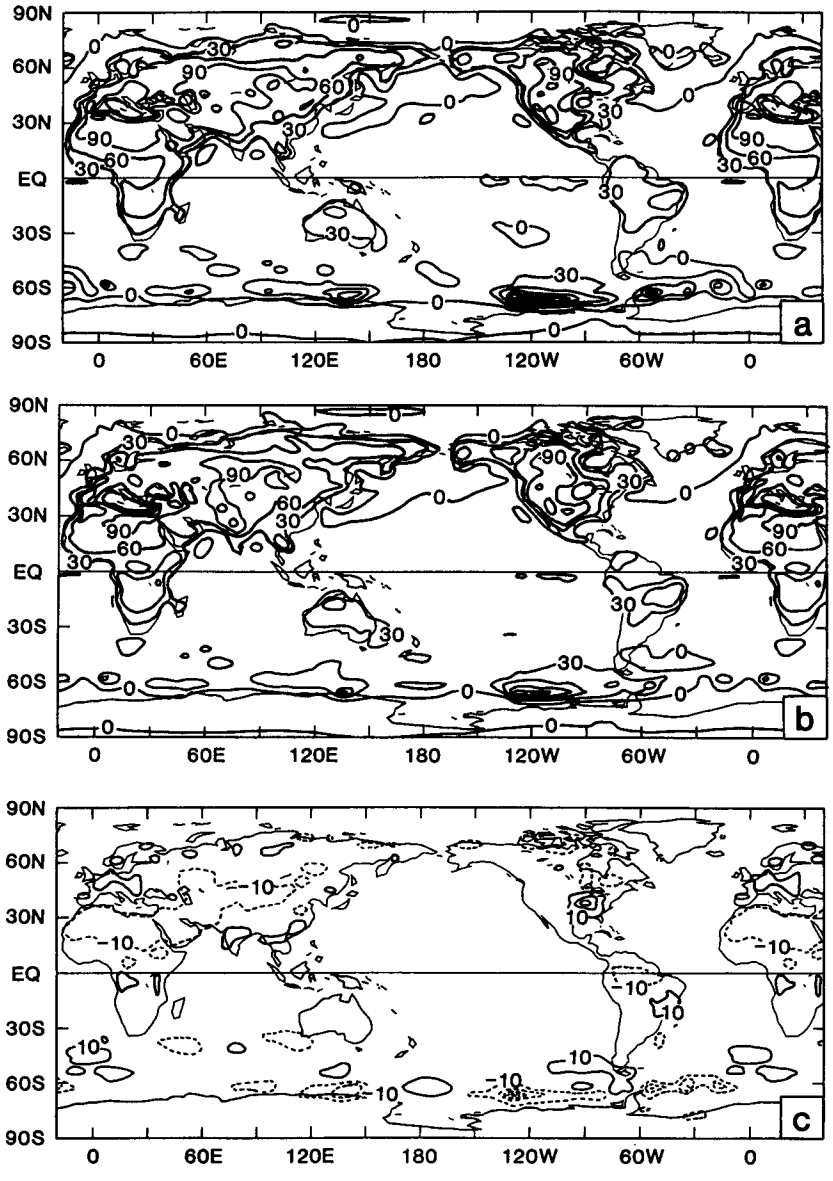

FIG. 11. (a) Global field of the mean sensible heat flux from surface in the SiB–GCM for the 15-day period (10–25 July). The contour interval is 25 W m^{-2}. (b) Same as in Fig. 11a, but for SSiB–GCM. (c) The difference of 15-day mean sensible heat flux from surface: SSiB–GCM minus SiB–GCM. The contour interval is 20 W m^{-2}.

wegian spruce observational data are used as forcing, and the surface vegetation is specified to be type 10, dwarf trees and shrubs with groundcover. The results shown are for three-month means. The figures show this difference is not very large. The rms difference is 2.4 W m^{-2} for the sensible heat flux, 3.23 W m^{-2} for the latent heat flux, and 0.025 m s^{-1} for friction velocity. Figure 10 shows the friction velocity in SSiB is lower than in SiB. The one story vegetation produces less eddy momentum transfer than the two stories.

Besides the experiments discussed above, additional tests have been carried out to validate SSiB under different circumstances. The results are shown in Table 4. Except for the Amazon and Norwegian tests, the forcing data were taken from GCM output. These results show that the monthly averages in SSiB are quite close to the SiB results in terms of sensible heat flux, latent heat release, and momentum exchange.

7. Experiments in a GCM

The SSiB was implemented into the COLA GCM (Kinter et al. 1988) following the method of Sato et al. (1989). This model was integrated from 10 July to 25 July 1983, and will be called Case 1. The average

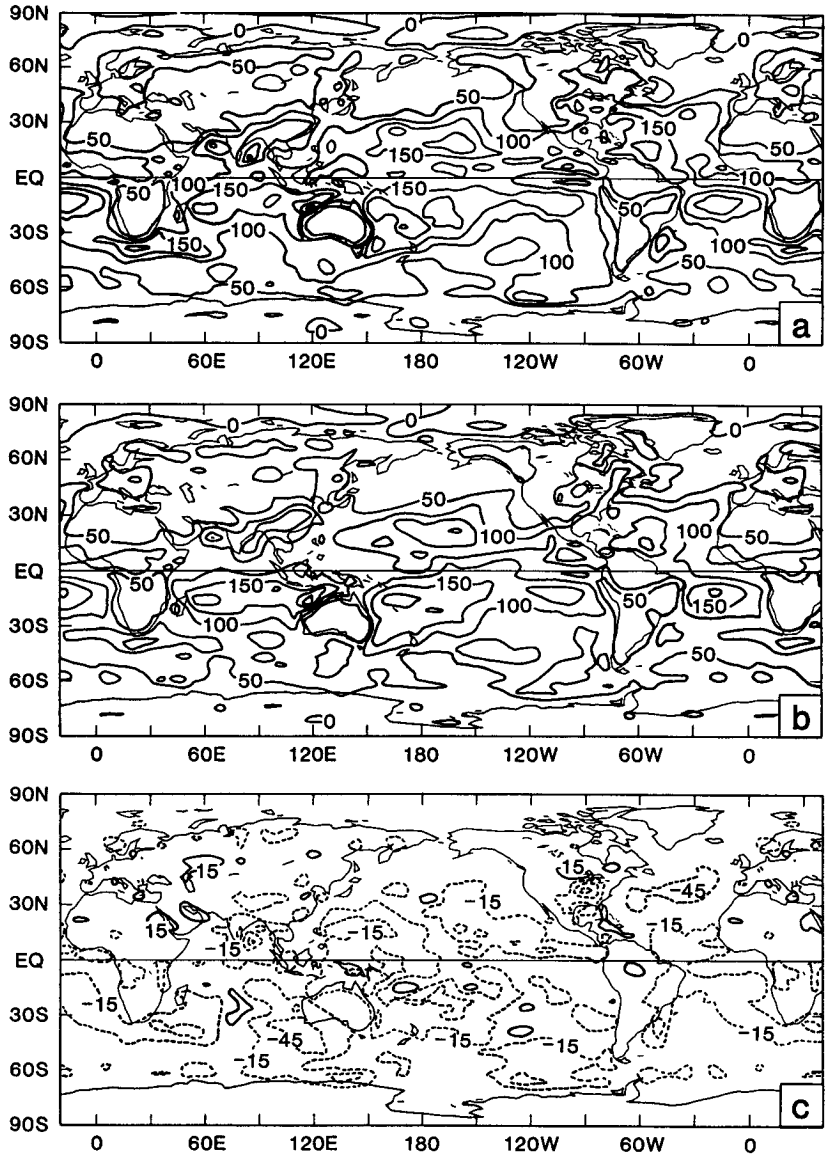

FIG. 12. (a) Global field of the mean latent heat flux from surface in the SiB–GCM for the 15-day period (10–25 July). The contour interval is 50 W m^{-2}. (b) Same as in Fig. 12a, but for SSiB-GCM. (c) The difference of the 15-day mean latent heat flux: SSiB–GCM minus SiB–GCM. The contour interval is 25 W m^{-2}.

of the 15 days was taken to compare with the previous results of Sato et al., which will be called Case 2. Since the results were obtained in Case 2, some improvements and corrections were made in both SiB and the GCM. In particular, the new vegetation dataset was used in SSiB. Therefore, the differences between Cases 1 and 2 should be considered as the maximum possible differences.

The differences of the 15-day means of surface temperature, sensible heat flux, and sea level pressure, and surface wind stress are small. Figure 11 shows the sensible heat flux, from Cases 1 and 2, and the differences between these two cases. There are no significant differences. The global means are about the same. Most of the regional differences may be random due to the small sample size rather than a direct consequence of simplification. The relatively large differences in the eastern part of the United States are caused by the changes of the SiB and the dataset after Sato et al.'s experiments.

Figures 12–14 show the results for latent heat flux, and precipitation. The application of SSiB leads to less evaporation, about 12% less than in SiB–GCM, and about 10.9 W m^{-2} in the global average. We attribute this to a replacement of the empirical scheme for computation of the Monin–Obukhov length used in Sato

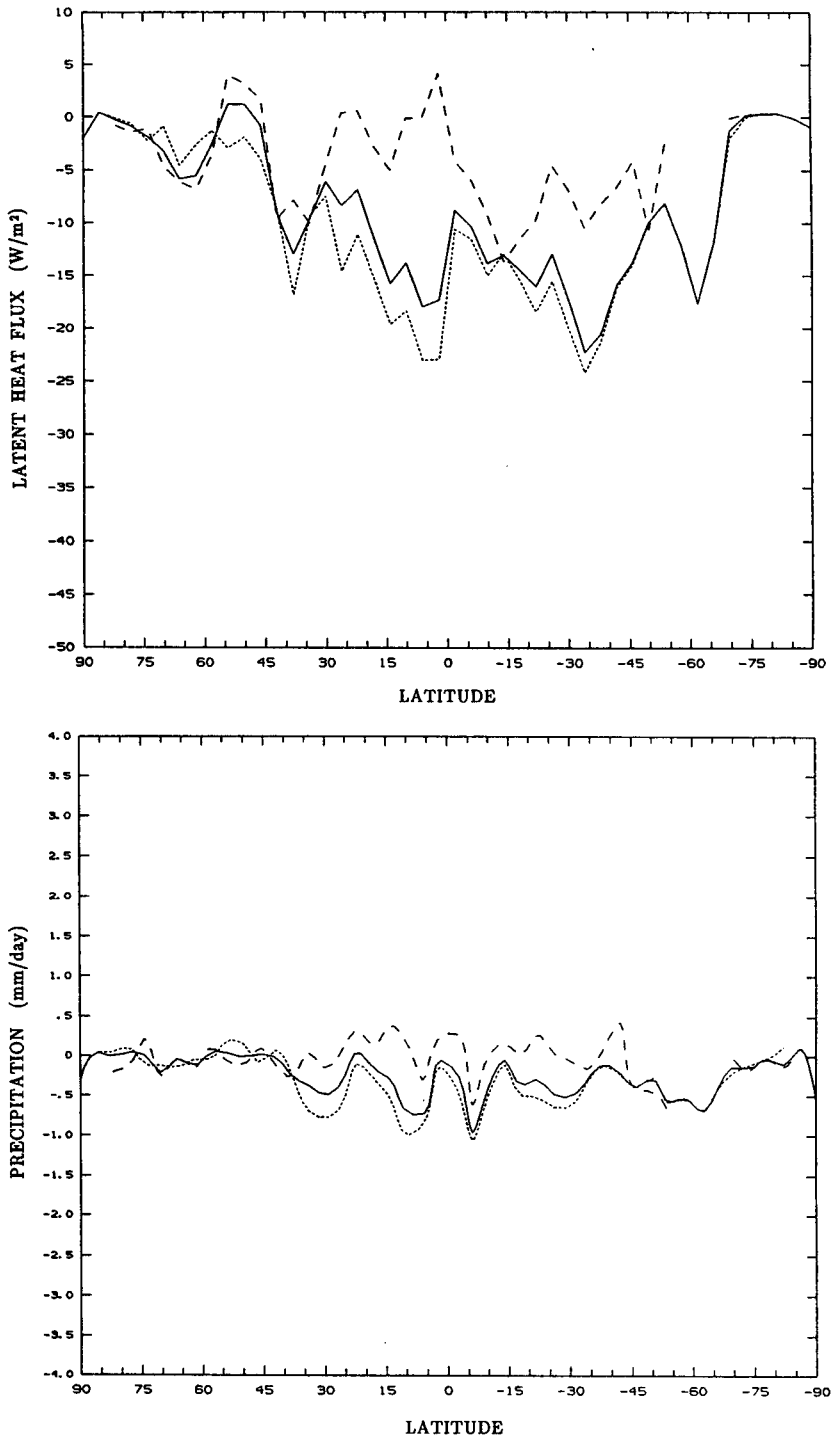

FIG. 13. (a) The difference of zonal average latent heat flux from surface for 15 day mean: SSiB–GCM minus SiB–GCM. Solid: total, dashed: land, dotted: ocean. (b) The difference of zonal average total precipitation for 15 day mean: SSiB–GCM minus SiB–GCM. Solid: total, dashed: land, dotted: ocean.

et al. (1989) by the Businger et al. (1971) and Paulson (1970) equations, which are supported by a large number of observations. This scheme is used over both land and ocean in the GCM. Figure 13a shows that the decrease of evaporation is present in most latitudes. The reduction is most significant over the ocean. Sato

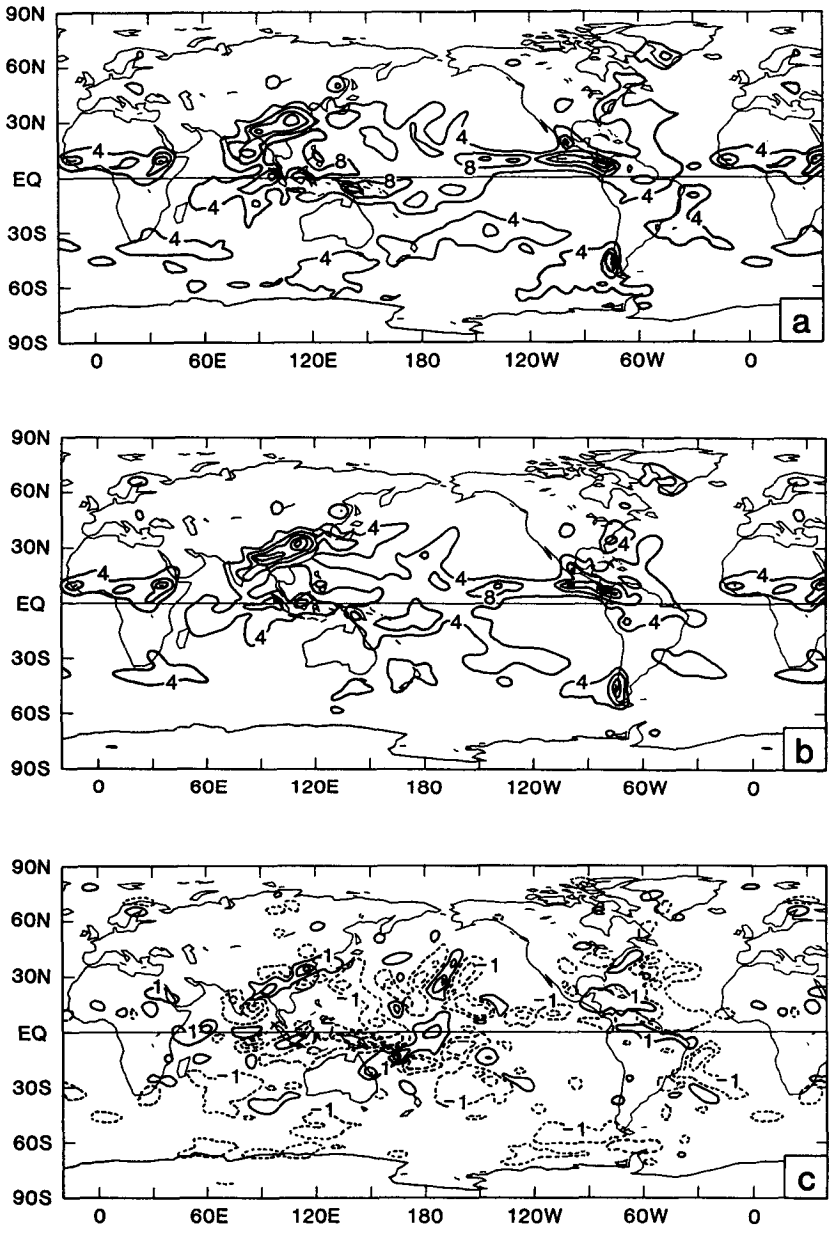

FIG. 14. (a) Global field of the total precipitation in the SiB–GCM for the fifteen day period (10–25 July). The contour interval is 4.3 mm day^{-1}. (b) Same as in Fig. 11a, but for SSiB–GCM. The contour interval is 4 mm day^{-1}. (c) The difference of 15-day total precipitation: SSiB–GCM minus SiB–GCM. The contour interval is 2 mm day^{-1}.

et al. (1989) mentioned that after the SiB implementation, the only place in the continental region which has the latent heat flux greater than 150 W m^{-2} is in South Asia. From Fig. 12c, we find that the latent heat flux decreases significantly in this region. In other land areas, the evaporation rate did not change as much.

The global mean precipitation is about 9% less in SSiB than SiB. Comparing Figs. 13a and 13b, we find the reduction of the evaporation rate over the continents does not lead to a corresponding reduction of precipitation there. The decrease of the precipitation is mainly over the oceans.

There are no large differences in zonal winds between the SSiB and SiB. This implies that GCM with SSiB has the same weakened tropospheric jet compared with the GCM without SiB found by Sato et al. (1989). A comparison of albedo differences (not shown) demonstrated that the global differences are very minor except for some spots near the North Pole when snow is melting. Since the albedo there is high and the ra-

diation flux is small, it would not affect the surface energy balance significantly.

8. Conclusions and discussions

In an effort to bridge the gap between the typical hydrological treatment of the land surface biosphere, which is very complex, and the conventional general circulation model treatment, which is specified through a single parameter, we have carried out a comprehensive analysis of the model of Sellers et al. (1986).

The radiation flux, turbulent transfer, and the energy partition at the surface are the most important processes in the surface layer. Every surface layer model has to seek some way to resolve these processes. In these respects, the SiB model provides a significant contribution for the calculation of surface albedo, aerodynamic resistance, and surface resistance. Our simplification of this model also focuses on these three parts. We have identified the most significant terms and variables in the model whose variations can affect the structure of the atmospheric boundary layer. In so doing, we have been able to reduce the number of free parameters in the SiB model by a factor of two. And, while there are still 21 parameters in the reduced set, many of these cannot be varied independently if a realistic parameter set is to be retained. As a result, the model is more suitable for general circulation sensitivity studies, given the more manageable size of the parameter set.

In the diurnal cycle of surface albedo computation we replace a complicated calculation by a harmonic fit. This parameterization made the model more efficient. As more sophisticated albedo models are developed and more observational data became available, we expect to further incorporate this information to have more reliable coefficients in the model.

The major reduction of parameters was affected by simplifying the soil moisture effect on stomatal resistance as well as an elimination of two story vegetation. In the remaining 21 parameters 14 are from vegetation.

While using the Businger and Paulson equations in the GCM we developed some equations which related the Richardson number to the aerodynamic resistance. The comparison showed that these relations are well simulated. Furthermore, the linear equations were introduced to simplify the calculation. The results turned out to be more successful than was expected.

We validated the reduced parameter model against both Sellers et al. (1986) and Sato et al. (1989) using zero- and three-dimensional versions of the model. We found that SSiB reproduced the major results of those two studies quite closely. Meanwhile, the parameterization of aerodynamic resistance calculation leads to a further decrease of evaporation rate in the GCM.

The SSiB, having fewer parameters which are physically easier to understand, represents a more suitable tool for climate sensitivity studies than more complex hydrological models. We intend to continue to apply observational data to refine the parameter ranges and utilize the SSiB for both deforestation and desertification studies in the near future.

Acknowledgments. This research was supported by NASA Grants NAGW-1269 and NAGW-557, and NSF Grant ATM-8713567. We would like to extend our gratitude to Dr. K. Miyakoda for his helpful comments and suggestions on this paper. We wish to thank Mike Fennessy and Larry Marx for their assistance in running GCM. Special thanks go to Marlene Schlichtig and to Sharon Busching for typing this paper.

APPENDIX

Main Equations of SSiB

There are seven prognostic equations in this model which can be regarded as a subset of the original SiB equation set. The equation for canopy temperature T_c is,

$$C_c \frac{\partial T_c}{\partial t} = R_{nc} - H_c - \lambda E_c \tag{A1}$$

where R_{nc} is the net radiation flux at surface, and H_c and λE_c are

$$H_c = \frac{2(T_c - T_a)}{r_b} \rho c_p \tag{A2}$$

$$\lambda E_c = (e_*(T_c) - e_a) \frac{\rho c_p}{\gamma} \left[\frac{W_c}{r_b} + \frac{1 - W_c}{r_b + r_c} \right] \tag{A3}$$

where T_a and e_a are temperature and vapor pressure in canopy air space, $e_*(T_c)$ is saturation vapor pressure at temperature T_c, W_c the wetness fraction of canopy, γ the psychrometric constant, and λ the latent heat of vaporization. The equation for ground temperature, T_{gs}, is

$$C_{gs} \frac{\partial T_{gs}}{\partial t} = R_{ngs} - H_{gs} - \lambda E_{gs} - \frac{2\pi C_{gs}}{\tau} (T_{gs} - T_d) \tag{A4}$$

where τ is the day length, C_{gs} the effective heat capacity of soil, T_d the temperature for deep soil, and H_{gs} and λE_{gs} are the sensible heat and latent heat fluxes from the ground defined by

$$H_{gs} = \frac{T_{gs} - T_a}{r_d} \rho c_p \tag{A5}$$

$$\lambda E_{gs} = [f_h e_{*(gs)} - e_a] \frac{\rho c_p}{\lambda} \frac{1}{r_{\text{surf}} + r_d} \tag{A6}$$

where f_h is the relative humidity of the air at the soil surface. The surface resistance is

$$r_{\text{surf}} = a_s(1 - w_1{}^{b_s}) \tag{A7}$$

where a_s and b_s are constants. The equation for deep soil temperature is T_d

$$C_{gs}\frac{\partial T_d}{\partial t} = 2(R_{ngs} - H_{gs} - \lambda E_{gs})/\sqrt{365\pi}. \tag{A8}$$

The governing equation for the canopy interception water store is

$$\frac{\partial M_c}{\partial t} = P_c - D_c - \frac{E_{wc}}{P_w} \tag{A9}$$

where P_c is the precipitation, D_c the water drainage rate (Sellers et al. 1986). An assumption of the distribution of precipitation at one grid point has been used to simulate a realistic runoff (Sato et al. 1989). The rate of evaporation from the wetted portions of the vegetation is

$$\lambda E_{wc} = \frac{[e(T_c) - e_a]}{r_b}\frac{\rho c_p}{\gamma}. \tag{A10}$$

Note that the equation for interception loss from ground cover has been eliminated. The governing equations for the soil wetness in the three soil layers are

$$\frac{\partial w_1}{\partial t} = \frac{1}{\theta_s D_1}\left[P_1 - Q_{12} - \frac{1}{P_w}(E_{gs} + b_1 E_{dc})\right] \tag{A11}$$

$$\frac{\partial w_2}{\partial t} = \frac{1}{\theta_s D_2}\left[Q_{12} - Q_{23} - \frac{1}{P_w} b_2 E_{dc}\right] \tag{A12}$$

$$\frac{\partial w_3}{\partial t} = \frac{1}{\theta_s D_3}[Q_{23} - Q_3] \tag{A13}$$

where the transpiration from soil is

$$\lambda E_{dc} = \frac{(e(T_c) - e_a)}{r_c + r_b}\frac{\rho c_p}{\gamma}(1 - w_c). \tag{A14}$$

The fraction factor b_i is

$$b_i = \frac{\text{root } l(i)}{\sum \text{root } l(i)} \tag{A15}$$

where root $l(i)$ is the root length at the ith layer, D_i the solid depth. The Q_{ij} is the transfer of water between ith and jth layers (Sellers et al. 1986), and θ_s is the volumetric soil moisture.

Temperature and water vapor pressure within the canopy air space are determined by the energy balance equations:

$$H_c + H_{gs} = \frac{T_a - T_r}{r_a}\rho c_p \tag{A16}$$

$$\lambda E_c + \lambda E_{gs} = \frac{e_a - e_r}{r_a}\frac{\rho c_p}{\gamma}. \tag{A17}$$

REFERENCES

Businger, J. A., J. C. Wyngaard, Y. Izumi and E. G. Bradley, 1971: Flux-profile relationships in the atmospheric surface layer. *J. Atmos. Sci.*, **28,** 181–189.

Charney, J. G., 1975: Dynamics of deserts and drought in the Sahel. *Quart. J. Roy. Meteor. Soc.*, **101,** 193–202.

——, W. J. Quirk, S. H. Chow and J. Kornfield, 1977: A comparative study of the effects of albedo change on drought in semi-arid regions. *J. Atmos. Sci.*, **34,** 1366–1385.

Dickinson, R. E., 1983: Land surface processes and climate-surface albedos and energy balance. *Advances in Geophysics.* Vol. 25, Academic Press, 305–353.

——, and A. Henderson-Sellers, 1988: Modelling tropical deforestation: A study of GCM land-surface parameterizations. *Quart. J. Roy. Meteor. Soc.*, **114,** 439–462.

——, ——, P. J. Kennedy and M. F. Wilson, 1986: Biosphere–atmosphere transfer scheme (BATS) for the NCAR community climate model. NCAR/TN − 275 + STR.

Dolman, A. J., 1988: Transpiration of an oak forest as predicted from porometer and weather data. *J. Hydrol.*, **97,** 225–234.

Dorman, J. L., and P. J. Sellers, 1989: A global climatology of albedo, roughness length and stomatal resistance for atmospheric general circulation models as represented by the Simple Biosphere Model (SiB). *J. Appl. Meteor.*, **28,** 833–855.

Federer, C. A., 1979: A soil-plant-atmosphere model for transpiration and availability of soil water. *Water Resour. Res.*, **153,** 555–562.

Garratt, J. R., 1978: Flux profile relations above tall vegetation. *Quart. J. Roy. Meteor. Soc.*, **104,** 199–211.

Goudriaan, J., 1977: Crop Micrometeorology: A simulation study. Wageningen Center for Agricultural Publishing and Documentation, 249 pp.

Jarvis, P. G., 1976: The interpretation of variations in leaf water potential and stomatal conductance found in canopies in the field. *Phil. Trans. Roy. Soc. London,* Ser. B., **273,** 593–610.

Kinter III, J. L., J. Shukla, L. Marx and E. K. Schneider, 1988: A simulation of the winter and summer circulations with the NMC global spectral model. *J. Atmos. Sci.*, **45,** 2486–2522.

Louis, J-F., 1979: A parametric model of vertical eddy fluxes in the atmosphere. *Bound.-Layer Meteorol.*, **17,** 187–202.

Manabe, S., 1969: The atmospheric circulation and hydrology of the earth's surface. *Mon. Wea. Rev.*, **97,** 739–774.

Matthews, E., 1985: *Atlas of archived vegetation, land-use and seasonal albedo data sets.* NASA Tech. Mem. 86199.

Mellor, G. L., and T. Yamada, 1982: Development of a turbulence closure model for geophysical fluid problems. *Rev. Geophys. Space Phys.*, **20,** 851–875.

Paulson, C. A., 1970: Mathematical representation of wind speed and temperature profiles in the unstable atmospheric surface layer. *J. Appl. Meteor.*, **9,** 857–861.

Rind, D., 1984: The influence of vegetation on the hydrologic cycle in a global climate model. *Climate Processes and Climate Sensitivity,* Monogr. 29. J. E. Hansen and T. Takahashi, Eds. Amer. Geophys. Union, 73–91.

Sato, N., P. J. Sellers, D. A. Randall, E. K. Schneider, J. Shukla, J. L. Kinter III, Y-T. Hou and E. Albertazzi, 1989: Effects of

implementing the Simple Biosphere Model in a General Circulation Model. *J. Atmos. Sci.*, **46**(18), 2757–2782.

Sellers, P. J., 1985: Canopy reflectance, photosynthesis and transpiration. *Int. J. Remote sens.*, **6**, 1335–1372.

——, and J. L. Dorman, 1987: Testing the Simple Biosphere Model (SiB) with point micrometeorological and biophysical data. *J. Climate Appl. Meteor.*, **26**(5), 622–651.

——, Y. Mintz, Y. C. Sud and A. Dalcher, 1986: A Simple Biosphere Model (SiB) for use within general circulation models. *J. Atmos. Sci.*, **43**, 505–531.

——, W. J. Shuttleworth, J. L. Dorman, A. Dalcher and J. M. Roberts, 1989: Calibrating the Simple Biosphere Model (SiB) for amazonian tropical forest using field and remote sensing data. Part 1: Average calibration with field data. *J. Appl. Meteor.*, **28**, 727–759.

Shukla, J., and Y. Mintz, 1982: Influence of land–surface evapotranspiration on the earth's climate. *Science*, **215**, 1498–1501.

——, C. Nobre and P. J. Sellers, 1990: Amazonia deforestation and climate change. *Science*, **215**, 1322–1325.

Stewart, J. B., 1988: Modelling surface conductance of pine forest. *Agric. Forest Meteor.*, **43**, 19–35.

Sud, Y. C., and W. E. Smith, 1984: Ensemble formulation of surface fluxes and improvement in evapotranspiration and cloud parameterization in a GCM. *Bound.-Layer Meteor.*, **29**, 185–210.

——, J. Shukla and Y. Mintz, 1988: Influence of land–surface roughness on atmospheric circulation and rainfall: A GCM sensitivity experiment. *J. Clim. Appl. Meteor.*, **27**, 1036–1054.

Szeicz, G., C. H. M. Van Bavel and S. Takami, 1973: Stomatal factor in the water use and dry matter production by sorghum. *Agric. Meteor.*, **12**, 361–389.

Xue, Y., K.-N. Liou and A. Kasahara, 1990: Investigation of the biogeophysical feedback on the African climate using a two-dimensional model. *J. Climate*, **3**, 337–352.